Materials Research Bulletin ***44****, 1899-1905 (2009)*

Structural phase transition in the perovskite-type tantalum oxynitrides, $Ca_{1-x}Eu_xTa(O,N)_3$

Teruki Motohashi[a]*, Yohei Hamade[a], Yuji Masubuchi[a], Takashi Takeda[a†], Kei-ichiro Murai[b], Akira Yoshiasa[c], Shinich Kikkawa[a]

[a] *Graduate School of Engineering, Hokkaido University, Sapporo 060-8628, Japan*
[b] *Department of Advanced Materials, University of Tokushima, Tokushima 770-8506, Japan*
[c] *Graduate School of Science and Technology, Kumamoto University, Kumamoto 860-8555, Japan*

Abstract

Pure $Ca_{1-x}Eu_xTa(O,N)_3$ were successfully synthesized in the whole range of Ca/Eu compositions by means of ammonia nitridation *via* a citrate precursor route. As-nitrided products with $x < 0.4$ were apparently orthorhombic, while those with $x \geq 0.4$ crystallized in a cubic structure. The anionic composition was found to be essentially O_2N and independent of Eu content (x). The as-nitrided $EuTaO_2N$ possessed a cubic perovskite-type structure, while high-temperature post-annealing led to a tetragonal $EuTaO_2N$ phase with better crystallinity. The re-nitridation transformed the post-annealed product into the original cubic lattice, which might be an average of the tetragonal micro domains.

*Corresponding author. Fax: +81(0)11 706 6740
E-mail address: t-mot@eng.hokudai.ac.jp (T. Motohashi)
[†]Present address: National Institute for Materials Science, 1-1 Namiki, Tsukuba, Ibaraki 305-0044, Japan.

1. Introduction

Oxynitrides have attracted increased attention due to their potential for various applications. In oxynitrides, two anion species, *i.e.* oxide and nitride anions coexist in the crystal lattice, leading to modifications in the cation-anion covalency, and thereby different electronic/optical properties from those in oxides. The more covalent nature of nitride anions than oxide anions results in smaller band gaps. Thus some oxynitrides are strongly colored and active to visible lights. Such unique properties make these materials promising candidates for photocatalysts for water splitting [1], nontoxic color pigments [2], and so on.

It has been known that oxynitrides also show intriguing structural characteristics. Indeed, the flexibility in anionic composition and distribution renders a rich variety in the crystal structure. For instance, gallium oxynitrides were reported to form at least three different structures, depending on their synthesis routes. A gallium oxynitride prepared by ammonolysis of amorphous oxide precursors crystallizes in a gallium-deficient wurzite-type structure $(Ga_{0.89}\square_{0.11})(N_{0.66}O_{0.34})$ [3,4], whereas that obtained from a ternary oxide $NiGa_2O_4$ forms a peculiar structure that is isomorphous to the carborundum II (B6-type or 6H-SiC) [5]. In addition, the Ga_3O_3N phase with a spinel structure was recently synthesized using an ultra high-pressure technique [6].

Another example concerns rare-earth tantalum oxynitrides *R*-Ta-(O,N). A comparative study on this class of materials revealed profound effects of the chemical composition on the crystal structure [7-9]. It was found that tantalum oxynitrides with larger rare-earths (R = Nd $\rightarrow$ Gd) crystallize in a pyrochlore-type structure $R_2Ta_2O_5N_2$, while a defect fluorite-type structure RTa(O,N,$\square$)$_4$ is stabilized for smaller rare-earths (R = Ho, Er, Yb, and Y) [7,8]. Interestingly, pyrochlore-type $R_2Ta_2O_5N_2$ (R = Nd, Sm, and Gd) is transformed into perovskite-type RTa(O,N)$_3$, when the sample is heavily nitrided by prolonged reaction duration [8]. These results clearly indicate that not only the cation size but also anionic composition play significant roles in determining the crystal structure. Nevertheless, the interplay between composition and structure has not been established for many oxynitride systems.

Transition-metal oxynitrides with a perovskite-type structure have been extensively investigated. Among them, alkali-earth-based tantalum oxynitrides were recently highlighted due to their unusual dielectric properties. Kim *et al.* reported [10] that

$BaTaO_2N$ and $SrTaO_2N$ exhibit bulk permittivity (κ) as large as 3,000 – 5,000 with moderate temperature coefficients. Importantly, the dielectric properties are strongly dependent on the kinds of alkali-earth elements: the bulk permittivity for $CaTaO_2N$ is much smaller (κ ≈ 30) than those for the Ba- and Sr-analogues [10]. $BaTaO_2N$ [11] and $CaTaO_2N$ [12] possess different crystallographic symmetries, *i.e.* the former and the latter crystallize in cubic *Pm*-3*m* and orthorhombic *Pnma*, respectively. Thus, it was argued that the dielectric properties seem to be related to the crystal structure. For $SrTaO_2N$, on the other hand, the situation is rather complicated. In previous reports, the crystal structure of $SrTaO_2N$ was refined based on three different space group, *i.e.* either tetragonal *I*4-2*m*, *I*4/*mcm*, or cubic *Pm*-3*m* [10,12-15]. These reports also reached discrepant conclusions in terms of preferential site occupation for O/N anions. The discrepancies imply that the crystal structure of $SrTaO_2N$ may depend on the synthesis condition. It has not been well understood what material parameters are predominant for determining the crystal structure of perovskite tantalum oxynitrides.

To address the issue on crystal chemistry of the perovskite oxynitrides, we focused on the europium tantalum oxynitride, $EuTa(O,N)_3$. This compound can be a structural reference for $SrTaO_2N$, since the ionic radius of Eu^{2+} (0.135 nm, C.N. = 10) is close to that of Sr^{2+} (0.136 nm, C.N. = 10; 0.144 nm, C.N. = 12) [16]. The preparation of $EuTa(O,N)_3$ was previously examined by Marchand *et al* [17]. They suggested that this compound possesses a cubic structure with the lattice parameter a = 0.4022 nm, but details in the structure and anion composition were not reported. Note that europium has two stable valence states, *i.e.* Eu^{2+} and Eu^{3+}, such that oxygen/nitrogen contents may be varied in $EuTa(O,N)_3$. In fact, a recent study by Jorge *et al.* revealed [18] that the compound tends to be nitrogen rich with respect to the "O_2N" composition. Such anionic nonstoichiometry is important, since the defect chemistries are suggested to play significant roles in the physical properties of europium-based oxynitride perovskites $EuMO_2N$ (*M* = Nb and Ta) [18]. They also reported that $EuTa(O,N)_3$ shows a slight tetragonal distortion. Nevertheless, it has remained unclear whether the anionic composition would have an impact on the crystal symmetry.

In the present study, the structure and anionic composition of $EuTa(O,N)_3$ were investigated. First we synthesized and characterized a series of the $Ca_{1-x}Eu_xTa(O,N)_3$ system in order to clarify how the properties are influenced upon substituting Eu for Ca^{2+} (0.123 nm, C.N. = 10; 0.134 nm, C.N. = 12). Then, we attempted high-temperature post-annealing on $EuTa(O,N)_3$ in order to improve the crystallinity by controlling the

structure and anionic composition.

2. Experimental

$Ca_{1-x}Eu_xTa(O,N)_3$ samples were synthesized by ammonia nitridation *via* a citrate precursor route. $CaCO_3$ (99.99%, Wako Pure Chemicals), Eu_2O_3 (99.9%, Aldrich), and $TaCl_5$ (99.99%, Aldrich) were used as starting materials. Stoichiometric amounts of these powders corresponding to 0.004 M of the final products were dissolved in 20 ml of anhydrous ethanol in which an equimolar amount of citric acid (98%, Wako Pure Chemicals) was added as a complexing agent. Since $TaCl_5$ is reactive with atmospheric moisture, the reagent was immediately weighed and dissolved in the ethanol solution to minimize the deterioration of the reagent. The solution was stirred and heated at 120°C to promote polymerization. Then the gelatinous product was prefired in air at 350°C for 1 hour, resulting in a brown solid residue. This solid was ground and placed in an alumina boat. The nitridation reaction was carried out at 1000°C for 15 hours in flowing ammonia (50 mL min^{-1}). After the ammonia nitridation, the sample was slowly cooled to room temperature under the same ammonia flow rate. For $EuTa(O,N)_3$, the as-nitrided powder was pelletized and then post-annealed at 1200°C for 15 hours in a quartz ampule evacuated to ~10^{-1} Pa, followed by furnace cooling to room temperature.

As-nitrided and post-annealed products were characterized by means of X-ray powder diffraction (XRD; Rigaku Ultima IV; CuKα radiation). The data were collected over the angular range of 10 – 120° with a step size of 0.02° and counting times of 1.0 – 2.0 sec per step. The crystal structure of the samples was refined using the Rietveld method with RIETAN2000 software [19]. The anionic composition was determined using an oxygen/nitrogen analyzer (Horiba EMGA-620W) from three parallel analyses. X-ray absorption of Eu L_{III}- and Ta L_{III}-edges was measured in transmission mode at the beam line 9C in Photon Factory, High Energy Accelerator Research Organization, Tsukuba. A small amount of the sample powder was sandwiched between Scotch tapes. $EuCl_2$, Eu_2O_3, Ta_3N_5, and Ta_2O_5 were used as references for Eu, and Ta, respectively.

Transmission electron microscope (TEM) observations were carried out with JEM-2100F (JEOL) to obtain electron diffraction (ED) patterns. The sample observed was in a powder form, ultrasonically dispersed in acetone, and deposited on a holey carbon film supported by a copper grid. Electrical resistivity was measured using the

van der Pauw method. The measurements were performed at room temperature with a four-probe apparatus (Toyo Co. ResiTest8300).

3. Results and discussion

3.1. Characterization of $Ca_{1-x}Eu_xTa(O,N)_3$

Figure 1 shows XRD patterns for as-nitrided products of $Ca_{1-x}Eu_xTa(O,N)_3$ with x = 0, 0.2, 0.4, 0.6, 0.8, and 1.0. All the products are well crystallized without any trace of secondary phases, indicating that $CaTa(O,N)_3$ and $EuTa(O,N)_3$ form a solid solution in the whole range of Ca/Eu compositions. For the Ca-end member (x = 0), diffraction peaks are readily indexed based on orthorhombic space group *Pnma* (so-called $GaFeO_3$-type structure), consistent with that previously reported [10,12,20]. Upon Eu substitution, double peaks at $2\theta \approx 40°$ [(220) and (022) peaks] and $\approx 57°$ [(240) and (042), (321) and (123) peaks] tend to merge into single peaks, reflecting a decreased orthorhombic distortion in Eu-rich compositions.

Lattice parameters were calculated for all the as-nitrided products assuming orthorhombic space group *Pnma*. In Fig. 2, the *a*-, *b*-, and *c*-axis lengths are plotted as a function of Eu content (x). With increasing x, all the lengths systematically expand, while the difference in the *a*- and *c*-axis lengths decreases. It appears that the slope of each plot abruptly changes at $x > 0.4$, suggesting that a structural transition takes place at $x \approx 0.4$. The crystal structure was refined for the samples with $x = 0.4 – 1.0$ assuming cubic space group *Pm*-3*m*. The refinements were successful yielding reasonably low *R*-values. The cubic reduced lattice parameter a_c linearly increases with increasing the Eu content, as shown in the inset of Fig. 2. From these results, the Eu-for-Ca substitution in $CaTa(O,N)_3$ was assumed to induce an orthorhombic-to-cubic transition at $x \approx 0.4$. Our as-nitrided $EuTa(O,N)_3$ product showed no apparent tetragonal distortions in the XRD pattern, contrary to the previous report by Jorge *et al.* [18]. The discrepancy in the crystal lattice may arise from different anionic compositions.

Oxygen and nitrogen contents of the as-nitrided products are summarized in Table 1. The data indicate that the anionic composition seems to be essentially "O_2N" for all the Ca/Eu compositions within the errors in this analysis. To reveal the valence states of Eu and Ta, X-ray absorption spectra were measured. The Eu L_{III}-edge XANES spectra consist of two peaks in all the Eu-containing products, as shown in Fig. 3. Since the

low-energy ($E \approx 6970$ eV) and high-energy ($E \approx 6980$ eV) peaks are similar to those for $EuCl_2$ and Eu_2O_3, the former and the latter are accordingly attributed to the $2p_{3/2} \rightarrow 5d$ transition of Eu^{2+} and Eu^{3+}, respectively, as in a previous literature [21]. Therefore, europium ions are in mixed valent between +2 and +3. The Eu^{3+} peak is large in $x = 0.2$ because its ionic size is small enough to occupy the Ca^{2+} site, while its intensity systematically decreases with increasing x. In $x = 1.0$ ($EuTaO_2N$), europium is mainly divalent with a small amount of trivalent species.

The Eu^{2+}/Eu^{3+} coexistence is easily explained if the Eu-containing products are assumed to be slightly off-stoichiometric with N-rich compositions. The presence of excess nitride anions in $EuTaO_2N$ was indeed reported in Ref. [18]. Another possible explanation is that tantalum is also mixed-valent between Ta^{4+} and Ta^{5+} so as to compensate extra positive charges of europium. The presence of tetravalent Ta is suggested by the result of electrical resistivity (ρ) measurements. The $CaTaO_2N$ phase is insulating with the ρ value of 3×10^6 Ω cm at room temperature, in good agreement with that previously reported [10]. For $EuTaO_2N$, on the other hand, the ρ value is ≈80 Ω cm, being five orders of magnitude smaller than that of $CaTaO_2N$. This is consistent with the fact that the color of $EuTaO_2N$ is significantly darkened as compared to $CaTaO_2N$ which is yellow green in color. The darkened sample color due to mixed-valent Ta was also reported for a dysprosium tantalum oxynitride prepared by ammonia nitridation at relatively higher temperatures [8]. It was not possible to determine the Ta valence by means of XANES spectroscopy without ambiguity, because the positions of L_{III}-edge are close to each other for Ta^{4+} and Ta^{5+} [22].

The present study has revealed that as-nitrided $EuTa(O,N)_3$ shows the following structural features: (1) this oxynitride crystallizes in a cubic perovskite structure and (2) the anionic composition is essentially O_2N. Nevertheless, with a careful look at the results of Rietveld refinement, the crystal structure of this compound seems to be more complex. The important crystallographic features and atomic parameters of $EuTaO_2N$ are summarized in Tables 2 and 3, respectively. In these tables, the data for $CaTaO_2N$ are also given. Because the two anions, *i.e.* oxygen and nitrogen, are indistinguishable by XRD analysis, no attempts were made to differentiate between them. $EuTaO_2N$ shows unusually large displacement parameters ($B = 2.1 \times 10^{-2}$ nm^2) for oxygen and nitrogen atoms, while the values for Eu and Ta atoms are reasonably small. A relatively large B value is also seen for the O/N(1) site in $CaTaO_2N$, but the feature is more remarkable in $EuTaO_2N$.

The large displacement is not dynamical but may be related to statistical distribution of O^{2-} and N^{3-}. Due to differences in the atomic distance and covalency of Ta-O and Ta-N bonds, oxygen and nitrogen atoms are displaced from the ideal perovskite site at (0, 0, 0.25). Two structural models are suggested to explain the large *B* values. In the first model, local atomic order is assumed to exist around Ta, whereas it occurs with an extremely small correlation length, resulting in the cubic symmetry as an average structure. The possibility of local atomic order has also been suggested for $BaTaO_2N$. A low-symmetry coordination geometry around Ta was indicated by EXAFS spectroscopy at the Ta L_{III}-edge [23] and pair distribution function analysis of the total neutron scattering [24], although the average structure as revealed by x-ray/neutron diffraction analyses is cubic *Pm*-3*m*. The second model is based on a micro-domain structure which is composed of randomly oriented regions with local symmetry lower than the average cubic. In fact, first-principles electronic-structure calculations by Wolff and Dronskowski indicated [25] that the cubic structure is energetically unfavorable for alkali-earth-based Ta/Nb oxynitride perovskites, and there is a clear preference of O/N atomic order which leads to a lowered symmetry. As discussed in the next section, this domain-structure model is more likely for the cubic $EuTaO_2N$ phase.

3.2. High-temperature annealing effects for $EuTaO_2N$

Figure 4 presents an XRD pattern for the post-annealed $EuTaO_2N$ product. Upon high-temperature annealing, diffraction peaks are sharpened, indicating a sign of improved crystallinity. It is also seen that several peaks at higher angles are clearly split [Fig. 4(b)], and a tiny extra peak appears at $2\theta \approx 37°$ [inset of Fig. 4(a)]. The profile of this extra peak is rather blurred, since its relative intensity is much smaller than the fundamental diffraction peaks (< 0.1%). These features are properly explained assuming a tetragonal superlattice with $\sqrt{2}a_c \times \sqrt{2}a_c \times 2a_c$ unit cell (a_c denotes the lattice parameter of cubic perovskites). All the diffraction peaks are accordingly indexed based on this structural model, as shown in Fig. 4. Among various oxide/oxynitride perovskites, only two symmetries, *i.e.* *P*4/*mbm* and *I*4/*mcm*, are applicable with this tetragonal superlattice [26]. The XRD pattern evidences the extinction rule with the relation of $h + k + l = 2n + 1$. Thus, the body-centered *I*4/*mcm* space group is more appropriate than *P*4/*mbm* to describe the structure of the post-annealed $EuTaO_2N$. Note that this space group is also assigned to the structure of $SrTaO_2N$. In this perovskite

structure, corner-shared $Ta(O,N)_6$ octahedra are rotated with respect to each other about the tetragonal *c*-axis.

The XRD pattern for the post-annealed $EuTaO_2N$ was successfully refined with the *I*4/*mcm* space group. Results of the refinement are summarized in Tables 4 and 5. The Ta-O/N bond distance and the Ta-O/N-Ta angle are similar to those reported for the isostructural $SrTaO_2N$ [10,12,15]. The distance along the *a*-axis [*i.e.* Ta-O/N(2)] is exactly the same as that in the as-nitrided product (0.201 nm), while the distance along the *c*-axis [*i.e.* Ta-O/N(1)] is slightly longer (0.202 nm). Since the Ta-N bond tends to be shorter than the Ta-O bond due to a stronger covalent character of nitrogen, the population of nitrogen is suggested to be lower at O/N(1) than O/N(2). Such preferential site occupations may cause the stabilization of the tetragonal structure. It is noticed that the displacement parameter of the O/N(1) site is large ($B = 2.8 \times 10^{-2}$ Å^2) due to the O/N coexistence at this site. The oxygen enrichment at the axial O/N(1) site was also reported for the isostructural niobium oxynitride, $SrNbO_2N$ [27].

Selected-area ED patterns were collected for the as-nitrided and post-annealed $EuTaO_2N$ to gain additional insight into this structural modification. Figure 5(a) is a representative ED pattern for the post-annealed product recorded with the incident electron beam along the $[101]_c$ direction of the cubic perovskite unit cell (denoted by a subscript "c"). In the ED pattern, extra spots are observed in addition to strong reflections of the fundamental perovskite structure. These extra spots reveal a body-centered superstructure, consistent with the XRD analysis (Fig. 4). The $[101]_c$ zone ED pattern for the as-nitrided product is shown in Fig. 5(b). Importantly, this ED pattern also displays similar extra spots which cannot be indexed on the primitive cubic unit cell. This implies that the local symmetry in the as-nitrided $EuTaO_2N$ does not agree with the average cubic symmetry as revealed by the XRD analysis.

The post-annealed $EuTaO_2N$ was fired again at 1000°C for 15 hours in flowing ammonia (50 mL min^{-1}). That is, the sample was "re-nitrided" with the same condition as the initial nitridation. As shown in Fig. 6, the re-nitrided product shows lowered crystallinity with no indication of tetragonal distortions, and its diffraction pattern is essentially identical to that of the as-nitrided product. The cubic lattice parameter was refined to be $a_c = 0.4020$ nm, which is comparable to that of the as-nitrided product. The fact that the crystallinity is deteriorated upon low-temperature re-nitridation is hard to be explained by simple annealing effects, suggesting that the re-nitridation process is

likely to involve variations in the chemical composition.

In fact, small differences in the oxygen and nitrogen contents were detected among the as-nitrided, post-annealed, and re-nitrided $EuTaO_2N$, although the anionic composition seems to be essentially O_2N in all the three products, as given in Table 6. The oxygen and nitrogen contents slightly increases (1.9 $\rightarrow$ 1.9 ~ 2.0) and decreases (1.0 $\rightarrow$ 0.8 ~ 0.9) in the post-annealed product, respectively, while they decreases (1.9 ~ 2.0 $\rightarrow$ 1.8) and increases (0.8 ~ 0.9 $\rightarrow$ 1.1) upon re-nitridation. During the post-annealing process, a part of nitride anions in the $EuTaO_2N$ phase was substituted by oxide anions from residual oxygen gas inside the quartz ampule. It is also suggested that the opposite substitution of O^{2-} to N^{3-} takes place during the re-nitridation process.

Taking into account the experimental fact that the post-annealed product exhibits the highest crystallinity, it would be reasonable to assume that the stoichiometric O_2N composition is realized in this product, while both the as-nitrided and re-nitrided products are slightly off-stoichiometric with N-rich "$O_{2-\delta}N_{1+\delta}$" compositions. Our structural analysis has revealed that $Ta(O,N)_6$ octahedra in the tetragonal $EuTaO_2N$ phase are slightly elongated along the *c*-axis (see Table 4). The longer Ta-O/N(1) distance along the *c*-axis is presumably due to lower concentration of nitride anions at the axial O/N(1) site. On the other hand, the deviation from the ideal O_2N composition would influence the coordination environment around Ta. One may anticipate that the $Ta(O,N)_6$ octahedra are less distorted, if oxide anions at the O/N(1) site are substituted by excess nitride anions. It is thus likely that the presence of excess nitride anions leads to the instability of long-range tetragonal order. We believe that the as-nitrided and re-nitrided products form a domain structure in nano or micron size with short-range tetragonal order. As a consequence, these products possess the cubic symmetry as an average structure, whereas a well-defined tetragonal order could exist in each domain, as evidenced by the selected-area ED analysis.

Similar micro-domain structures were observed for complex metal oxides such as fluorite-type ZrO_2-Y_2O_3 [28], ZrO_2-Gd_2O_3 [29], and perovskite-type $(La,Sr)(Ga,Mg)O_{3-\delta}$ [30,31]. In the latter case, neutron diffraction revealed cubic symmetry but electron diffraction showed the presence of a micro-domain structure which is composed of randomly oriented regions with local symmetry lower than the average cubic. The Rietveld refinement resulted in large displacement parameters for the oxygen atoms, indicating that on average the oxygen atoms are displayed away from

the ideal position in the cubic perovskite structure [30]. This feature is indeed similar to what was observed for the as-nitrided $EuTaO_2N$. Our compositional analysis suggested that approximately one excess nitrogen atom substitutes oxygen in every ten formula units of the cubic $EuTaO_2N$ phase. Assuming that such an excess nitrogen atom always disturbs the long-range tetragonal order, the domain structure should be very fine, *i.e.* the domain size being as small as ~1 nm in diameter.

The recent study by Jorge *et al.* [18] highlighted notable magneto-responses in the niobium oxynitride perovskite $EuNbO_2N$ that is isostructural to $EuTaO_2N$. This niobium oxynitride showed colossal (>99%) magnetoresistances and an apparent giant (20%) magnetocapacitance at low temperatures. The latter response was assumed to be microstructural effects, rather than an intrinsic multiferroism. The microstructure observed in the present study for $EuTaO_2N$ may be related to that of $EuNbO_2N$.

4. Conclusions

The perovskite-type tantalum oxynitrides $Ca_{1-x}Eu_xTa(O,N)_3$ ($0 \leq x \leq 1$) were synthesized, and their crystal structure and anionic composition were investigated. As-nitrided products with $x < 0.4$ were apparently orthorhombic, while those with $x \geq 0.4$ were assumed to crystallize in a cubic structure. The anionic composition was found to be essentially "O_2N" and independent of Eu content (x). High-temperature post-annealing of the as-nitrided $EuTaO_2N$ led to a tetragonal phase with better crystallinity. The selected-area electron diffraction analysis evidenced that the as-nitrided $EuTaO_2N$ possessed local symmetry lower than the average cubic crystal lattice. The compositional analysis suggested that the as-nitrided product is slightly off-stoichiometric with an N-rich "$O_{2-\delta}N_{1+\delta}$" composition which might lead to the instability of long-range tetragonal order.

Acknowledgment

The present work was supported by a Grant-in-Aid for Scientific Research (B) from the Japan Society for the Promotion of Science (Contract No. 19350098). The X-ray absorption experiments were performed under the approval of the Photon Factory Advisory Committee (Proposal No. 2007G554). T. M. acknowledges financial support

from the Global COE Program (Project No. B01: “Catalysis as the Basis for Innovation in Materials Science”) from the Ministry of Education, Culture, Sports, Science and Technology, Japan.

References

[1] M. Higashi, R. Abe, K. Teramura, T. Takata, B. Ohtani, and K. Domen, *Chem. Phys. Let.* **452**, 120 (2008).
[2] M. Jansen and H. P. Letschert, *Nature* **404**, 981 (2000).
[3] S. Kikkawa, K. Nagasaka, T. Takeda, M. Bailey, T. Sakurai, and Y. Miyamoto, *J. Solid State Chem.* **180**, 1984 (2007).
[4] S. Kikkawa, S. Ohtaki, T. Takeda, A. Yoshiasa, T. Sakurai, and Y. Miyamoto, *J. Alloys. Compds.* **450**, 152 (2008).
[5] X. Cailleaux, M. C. Marco de Lucas, O. Merdrignac-Conanec, F. Tessier, K. Nagasaka, and S. Kikkawa, *J. Phys. D: Appl. Phys.* **42**, 045408 (2009).
[6] E. Soignard, D. Machon, P. F. McMillan, J. Dong, B. Xu, and K. Leinenweber, *Chem. Mater.* **17**, 5465 (2005).
[7] F. Por, R. Marchand, and Y. Laurent, *J. Solid State Chem.* **107**, 39 (1993).
[8] P. Maillard, F. Tessier, E. Orhan, F. Cheviré, and R. Marchand, *Chem. Mater.* **17**, 152 (2005).
[9] S. Kikkawa, T. Takeda, A. Yoshiasa, P. Maillard, F. Tessier, *Mater. Res. Bull.* 43, 811 (2008).
[10] Y.- I. Kim, P. M. Woodward, K. Z. Baba-Kishi and C. W. Tai, *Chem. Mater.* **16**, 1267 (2004).
[11] F. Por, R. Marchand, Y. Laurent, P. Batcher, G. Roult, *Mater. Res. Bull.* **23**, 1447 (1988).
[12] E. Gunther and R. Hagenmayer, and M. Jansen, *Z. Anorg. Allg. Chem.* **626**, 1519 (2000).
[13] R. Marchand, F. Pors, and Y. Laurent, *Rev. Int. Hautes Temp. Refractaires*, **23**, 11 (1986).
[14] F. Pors, P. Bacher, R. Marchand, Y. Laurent, and G. Roult, *Rev. Int. Hautes Temp*. **24**, 239 (1987).
[15] S. J. Clarke, K. A. Hardstone, C. W. Michie, and M. J. Rosseinsky, *Chem. Mater.* **14**, 2664 (2002).
[16] R. D. Shannon, *Acta Cryst.* **A32**, 751 (1976).

[17] R. Marchand, F. Pors, and Y. Laurent, *Ann. Chim. Fr.* **16**, 553 (1991).
[18] A. B. Jorge, J. Oró-Solé, A. M. Bea, N. Mufti, T. T. M. Palstra, J. A. Rodgers, J. P. Attfield, and A. Fuertes, *J. Am. Chem. Soc.* **130**, 12572 (2008).
[19] F. Izumi and T. Ikeda, *Mater. Sci. Forum*, **321-324**, 198-203 (2000).
[20] A. Rachel, S. G. Ebbinghaus, M. Güngerich, P. J. Klar, J. Hanss, A. Weidenkaff, and A. Reller, *Thermochimica Acta* **438,** 134 (2005).
[21] Y. Takahashi, G. R. Kolonin, G. P. Shironosova, I. I. Kupriyanova, T. Uruga, and H. Shimizu, *Mineralogical Magazine* **69**, 179 (2005).
[22] S. Nemana and B. C. Gates, *J. Phys. Chem. B* **110**, 17546 (2006).
[23] B. Ravel, Y.- I. Kim, P. M. Woodward, and C.M. Fang, *Phys. Rev. B* **73**, 184121 (2006).
[24] K. Page, M. W. Stoltzfus, Y.- I. Kim, T. Proffen, P. M. Woodward, A. K. Cheetham and Ram Seshadri, *Chem. Mater.* **19**, 4037 (2007).
[25] H. Wolff and R. Dronskowski, *J. Comput. Chem.* **29**, 2260 (2008).
[26] R. H. Mitchell, in *Perovskites Modern and Ancient* (Almaz Press, Ontario, Canada, (2002).
[27] S. G. Ebbinghaus, A. Weidenkaff, A. Rachel, and A. Reller, *Acta Cryst. C* **60**, i91 (2004).
[28] S. Suzuki, M. Tanaka, and M. Ishigame, *Jpn. J. Appl. Phys.* **24**, 401 (1985).
[29] T. Uehara, K. Koto, F. Kanamaru, and H. Horiuchi, *Solid State Ionics* **23**, 137 (1987).
[30] A. Skowron, P.-N. Huang, and A. Petric, *J. Solid State Chem.* **143**, 202 (1999).
[31] T. Mathews and J. R. Sellar, *Solid State Ionics* **135**, 411 (2000).

Table 1. Oxygen and nitrogen contents of the as-nitrided $Ca_{1-x}Eu_xTa(O,N)_3$ products.

Eu content (x)	O / wt%	N / wt%	anionic composition*
0	11.2 ± 0.2	5.2 ± 0.3	$O_{1.9}N_{1.0}$
0.2	10.0 ± 0.3	5.1 ± 0.2	$O_{1.8}N_{1.0}$
0.4	9.7 ± 0.1	5.2 ± 0.3	$O_{1.9}N_{1.1}$
0.6	9.1 ± 0.1	4.8 ± 0.3	$O_{1.9}N_{1.1}$
0.8	8.4 ± 0.4	4.2 ± 0.1	$O_{1.9}N_{1.1}$
1.0	8.1 ± 0.3	3.7 ± 0.1	$O_{1.9}N_{1.0}$

*The cationic composition was assumed to be the same as that of the starting mixture.

Table 2. Rietveld refinement details for the as-nitrided products of $EuTaO_2N$ and $CaTaO_2N$.

	$EuTaO_2N$	$CaTaO_2N$
crystal system	cubic	orthorhombic
space group	*Pm*-3*m*	*Pnma*
a (nm)	0.40195(1)	0.56134(2)
b (nm)	–	0.78861(3)
c (nm)	–	0.55472(2)
volume (10^{-27} m^3)	0.064941(1)	0.24556(1)
$d_{Ta\text{-}O/N}$ (nm)	(6×) 0.201	(2×) 0.201
		(2×) 0.202
		(2×) 0.203
$d_{Ca/Eu\text{-}O/N}$ (nm)	(12×) 0.284	(2×) 0.312
		(1×) 0.245
		(1×) 0.261
		(2×) 0.305
		(2×) 0.306
		(2×) 0.239
		(2×) 0.275
∠ Ta-O/N-Ta (deg.)	(3×) 180	(1×) 153.6
		(2×) 156.1
R_{wp}	8.56	7.76
S	1.28	1.36
Z	1	4

Table 3. Atomic parameters for the as-nitrided products of $EuTaO_2N$ and $CaTaO_2N$.

atom	*g*	*x*	*y*	*z*	*B* (10^{-2} nm^2)
			$EuTaO_2N$		
Eu	1.0	0	0	0	0.75(2)
Ta	1.0	0.5	0.5	0.5	0.39(2)
O/N	0.67/0.33	0	0	0.25	2.1(2)
			$CaTaO_2N$		
Ca	1.0	0.026(1)	0.25	-0.022(1)	0.53(1)
Ta	1.0	0.5	0	0	0.38(2)
O/N(1)	0.67/0.33	0.48(0)	0.25	0.083(4)	1.3(6)
O/N(2)	0.67/0.33	0.29(0)	-0.028(3)	0.71(0)	0.5(4)

Table 4. Rietveld refinement details for the post-annealed $EuTaO_2N$.

	$EuTaO_2N$
crystal system	tetragonal
space group	*I*4/*mcm*
a (nm)	0.56829(1)
c (nm)	0.80620(1)
volume (10^{-27} m^3)	0.26036(1)
$d_{Ta\text{-}O/N}$ (nm)	(2×) 0.202
	(4×) 0.201
$d_{Eu\text{-}O/N}$ (nm)	(4×) 0.274
	(4×) 0.284
	(4×) 0.295
∠ Ta-O/N-Ta (deg.)	(3×) 171.4
R_{wp}	15.69
S	2.01
Z	4

Table 5. Atomic parameters for the post-annealed $EuTaO_2N$.

atom	*g*	*x*	*y*	*z*	*B* (10^{-2} nm^2)
Eu	1.0	0	0.5	0.25	0.65(4)
Ta	1.0	0.5	0.5	0	0.25(3)
O/N(1)	0.67/0.33	0	0	0.25	2.8(8)
O/N(2)	0.67/0.33	0.774(2)	1.274(2)	0	0.81(0)

Table 6. Oxygen and nitrogen contents of the as-nitrided, post-annealed, and re-nitrided products of $EuTa(O,N)_3$. The analyses were carried out for two parallel sample batches.

Sample batch	Products	O / wt%	N / wt%	anionic composition*
#1	as-nitrided	8.1 ± 0.3	3.7 ± 0.1	$O_{1.9}N_{1.0}$
	post-annealed	8.1 ± 0.3	3.4 ± 0.1	$O_{1.9}N_{0.9}$
	re-nitrided	7.4 ± 0.1	3.8 ± 0.1	$O_{1.8}N_{1.1}$
#2	as-nitrided	8.1 ± 0.3	3.7 ± 0.1	$O_{1.9}N_{1.0}$
	post-annealed	8.4 ± 0.4	3.4 ± 0.1	$O_{2.0}N_{0.8}$
	re-nitrided	7.5 ± 0.1	3.8 ± 0.1	$O_{1.8}N_{1.1}$

*The cationic composition was assumed to be the same as that of the starting mixture.

Figure captions

Fig. 1.

X-ray powder diffraction patterns for the as-nitrided products of $Ca_{1-x}Eu_xTa(O,N)_3$ with x = 0, 0.2, 0.4, 0.6, 0.8, and 1.0. For x = 0 [$CaTa(O,N)_3$] and 1.0 [$EuTa(O,N)_3$], diffraction peaks were indexed based on orthorhombic *Pnma* and cubic *Pm*-3*m* space groups, respectively.

Fig. 2.

The orthorhombic *a*-, *b*-, and *c*-axis lengths for the as-nitrided $Ca_{1-x}Eu_xTa(O,N)_3$ with respect to the Eu content (x). The inset represents the cubic reduced lattice parameter a_c refined based on *Pm*-3*m* space group.

Fig. 3.

Eu L_{III}-edge XANES spectra of the as-nitrided $Ca_{1-x}Eu_xTa(O,N)_3$ with x = 0.2, 0.4, 0.6, 0.8, and 1.0. The reference spectra of Eu_2O_3 (Eu^{3+}) and $EuCl_2$ (Eu^{2+}) are also shown.

Fig. 4.

(a) X-ray powder diffraction pattern for the post-annealed $EuTaO_2N$. The magnified pattern at 2θ = 36 – 40° is presented in the inset. (b) The magnified pattern at 2θ = 95 – 120°. In all the figures, diffraction peaks were indexed based on a tetragonal superstructure with $\sqrt{2}a_c \times \sqrt{2}a_c \times 2a_c$ unit cell (a_c denotes the lattice parameter of cubic perovskites).

Fig. 5.

Selected-area electron diffraction (ED) patterns. (a) The $[101]_c$ zone ED pattern for the post-annealed $EuTaO_2N$. (b) The $[101]_c$ zone ED pattern for the as-nitrided $EuTaO_2N$. Extra spots, which cannot be indexed on the primitive cubic unit cell, are indicated with arrows.

Fig. 6.

(a) X-ray powder diffraction patterns for the as-nitrided, post-annealed, and re-nitrided products of $EuTaO_2N$. (b) The magnified patterns at 2θ = 95 – 120°.

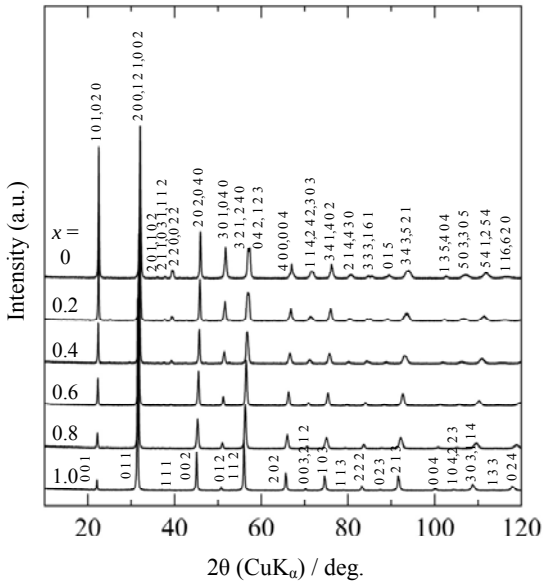

Fig. 1. Motohashi *et al.*

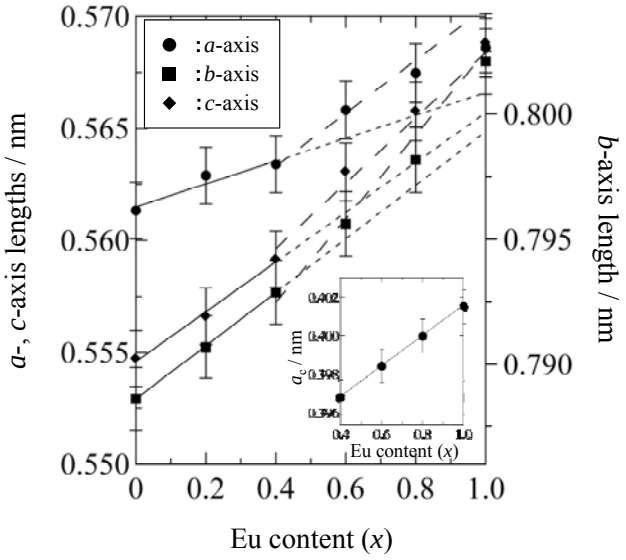

Fig. 2. Motohashi *et al.*

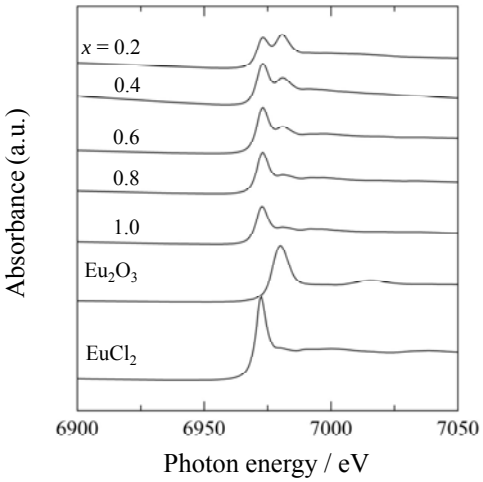

Fig. 3. Motohashi *et al.*

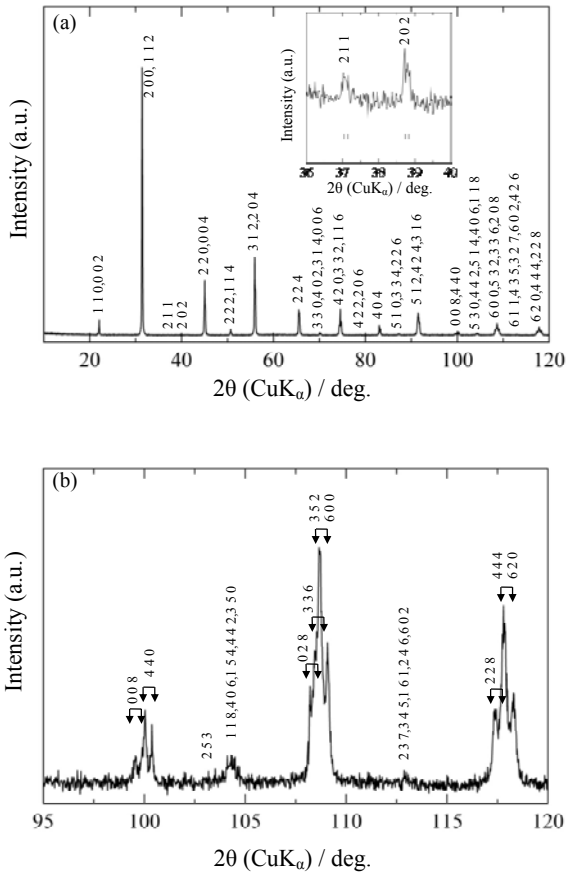

Fig. 4. Motohashi *et al.*

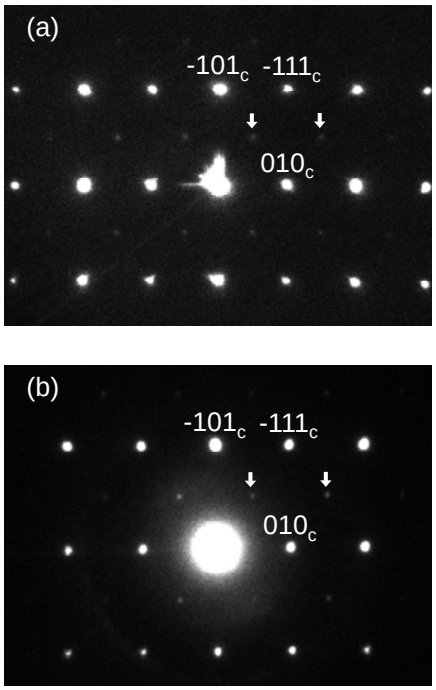

Fig. 5. Motohashi *et al.*

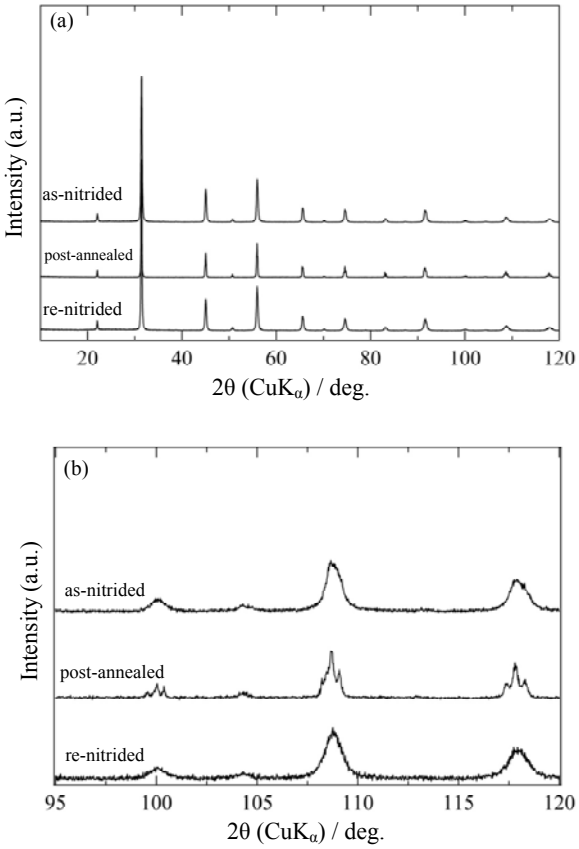

Fig. 6. Motohashi *et al.*